

Cyano-bridged {Fe^{III}Ln^{III}} heterobimetallic chains assembled through the [Fe^{III}{HB(pz)₃}(CN)₃]⁻ complex as metalloligand: Synthesis, crystal structure and magnetic properties

*Diana Visinescu,^{*a} Maria-Gabriela Alexandru,^{*b} Dan G. Dumitrescu,^c Sergiu Shova,^d
Nicolás Moliner,^e Francesc Lloret^e and Miguel Julve^{*e}*

^aCoordination and Supramolecular Chemistry Laboratory, “Ilie Murgulescu” Institute of Physical Chemistry, Romanian Academy, Splaiul Independentei 202, Bucharest 060021, Romania.

^bDepartment of Inorganic Chemistry, Physical Chemistry and Electrochemistry, Faculty of Applied Chemistry and Materials Science, University Politehnica of Bucharest, 1-7 Gh. Polizu Street, 011061 Bucharest, Romania, e-mail: alexandru.gabriela@gmail.com

^cElettra Sincrotrone Trieste SCpA, Str Statale 14, Km 163,5 AREA Sci Pk, I-34149 Trieste, Basovizza, Italy

^d“Petru Poni” Institute of Macromolecular Chemistry, Romanian Academy, Aleea Grigore Ghica Vodă 41-A, RO-700487 Iasi, Romania

^e Departament de Química Inorgànica/Instituto de Ciencia Molecular, Universitat de València, C/ Catedrático José Beltrán 2, 46980 Paterna, València, Spain. E-mail: miguel.julve@uv.es

Electronic Supplementary Information
(ESI)

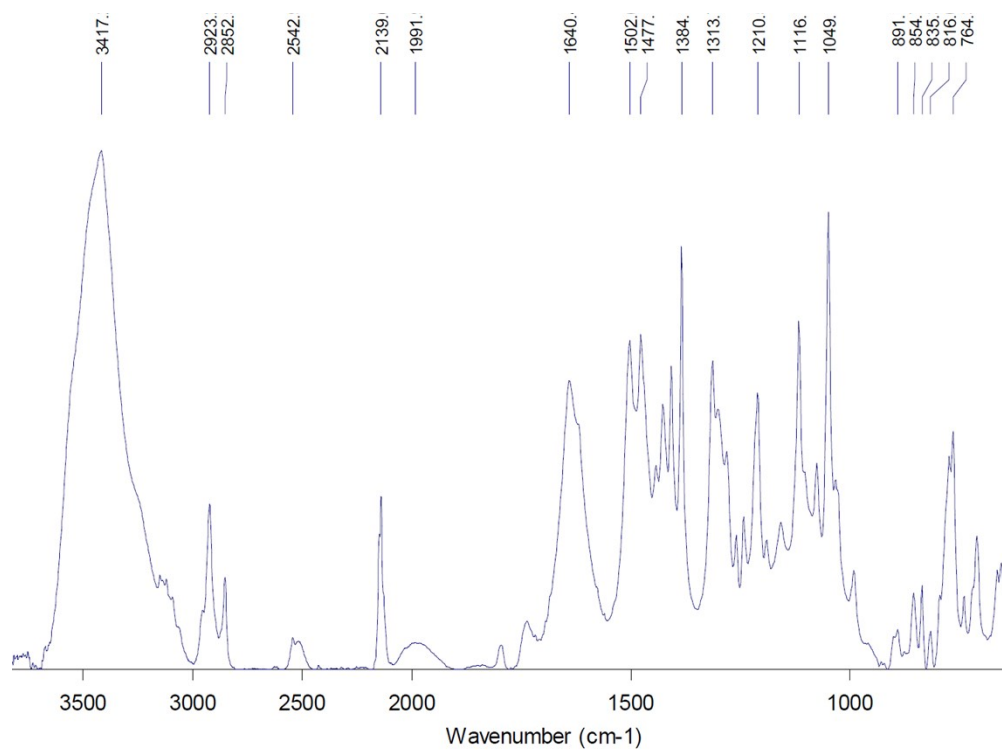


Fig. S1. FTIR spectrum for **1**.

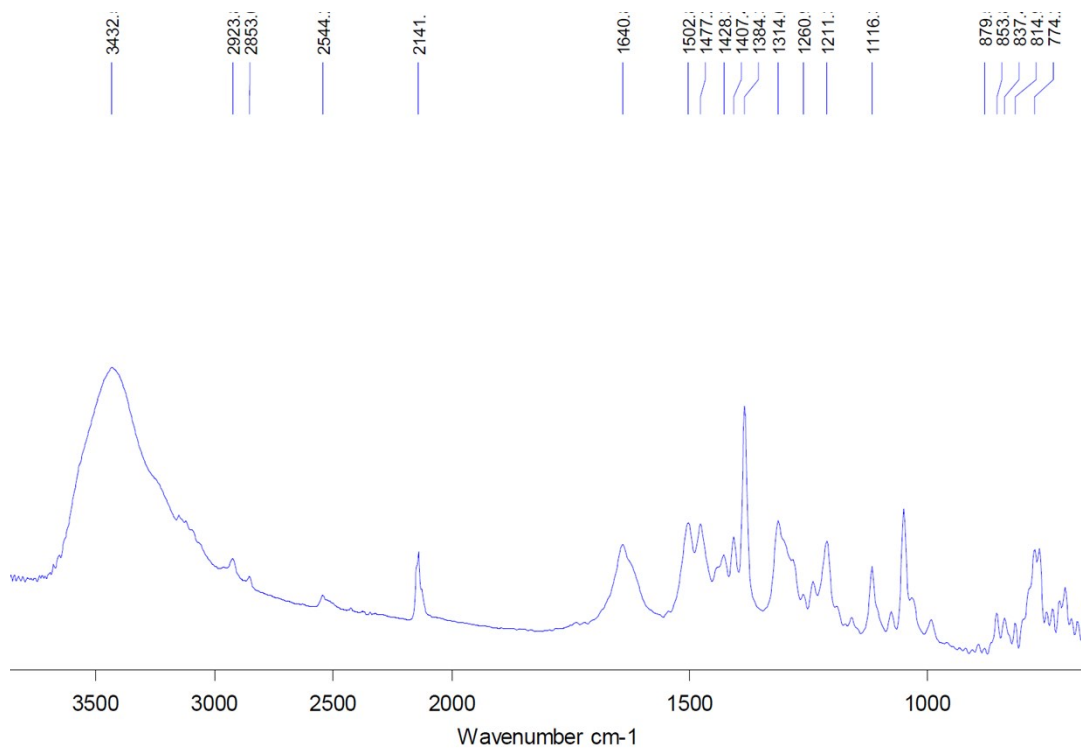


Fig. S2. FTIR spectrum for **2**.

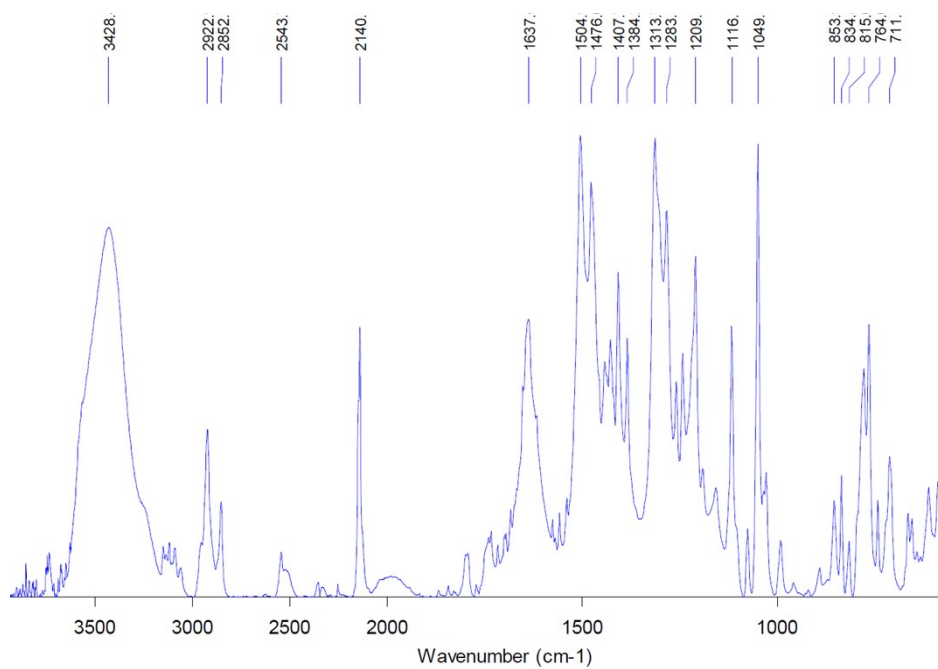


Fig. S3. FTIR spectrum for **3**.

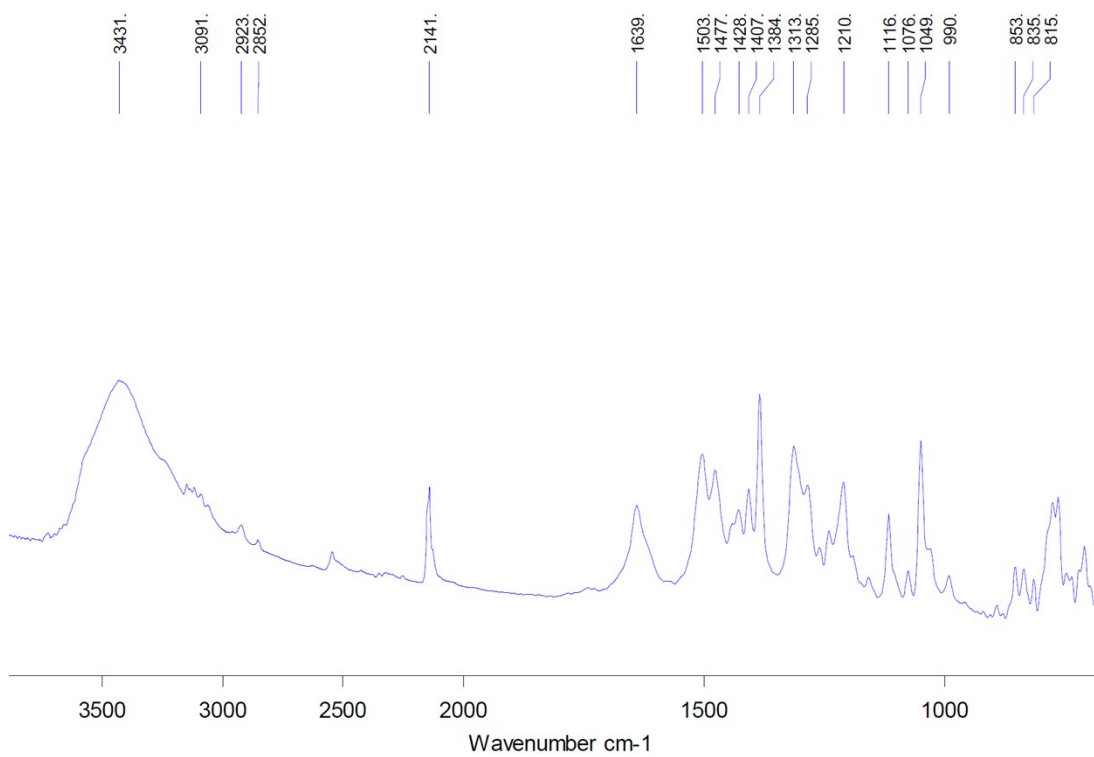


Fig. S4. FTIR spectrum for **4**.

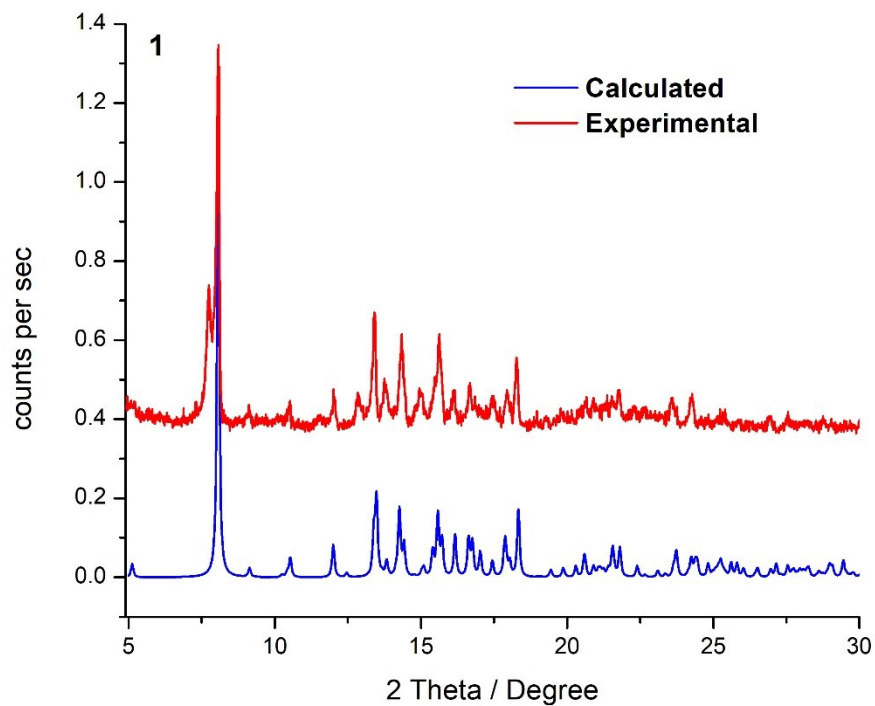


Fig. S5. Experimental and calculated PXR D at room temperature for **1**.

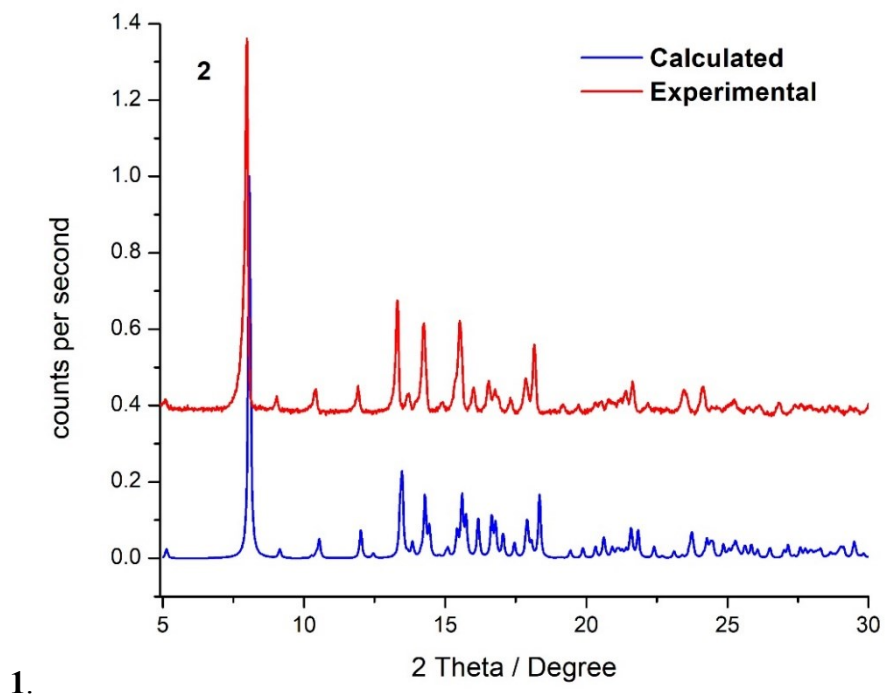


Fig. S6. Experimental and calculated PXR D at room temperature for **2**.

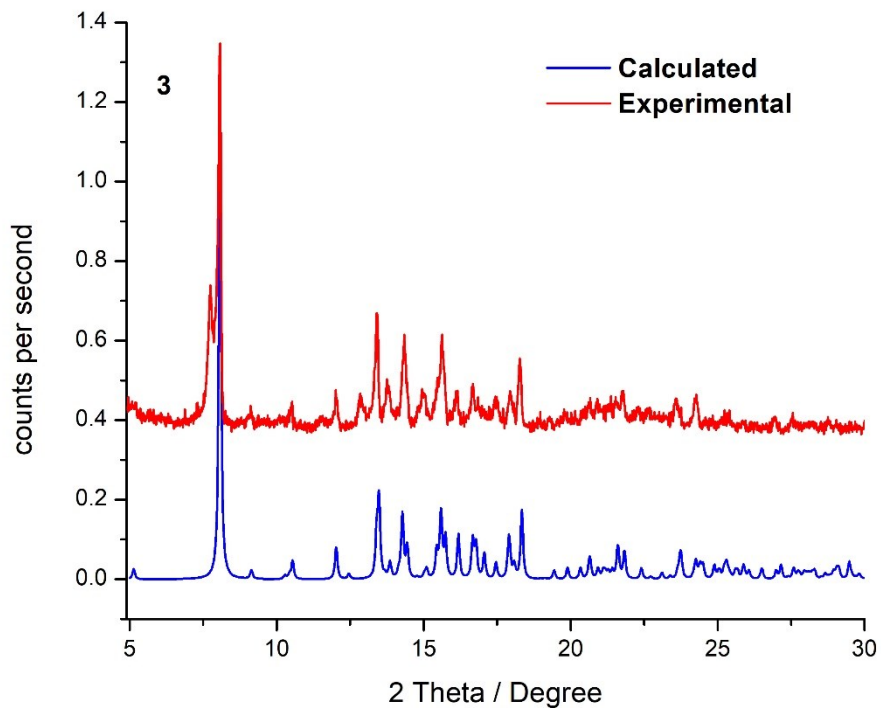


Fig. S7. Experimental and calculated PXRD at room temperature for **3**.

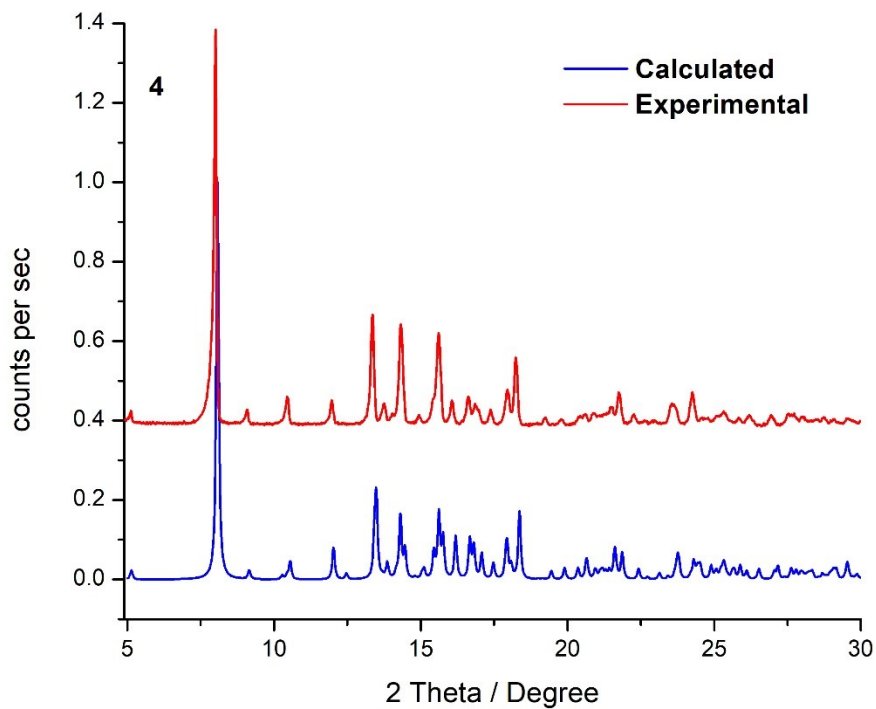


Fig. S8. Experimental and calculated PXRD at room temperature for **4**.

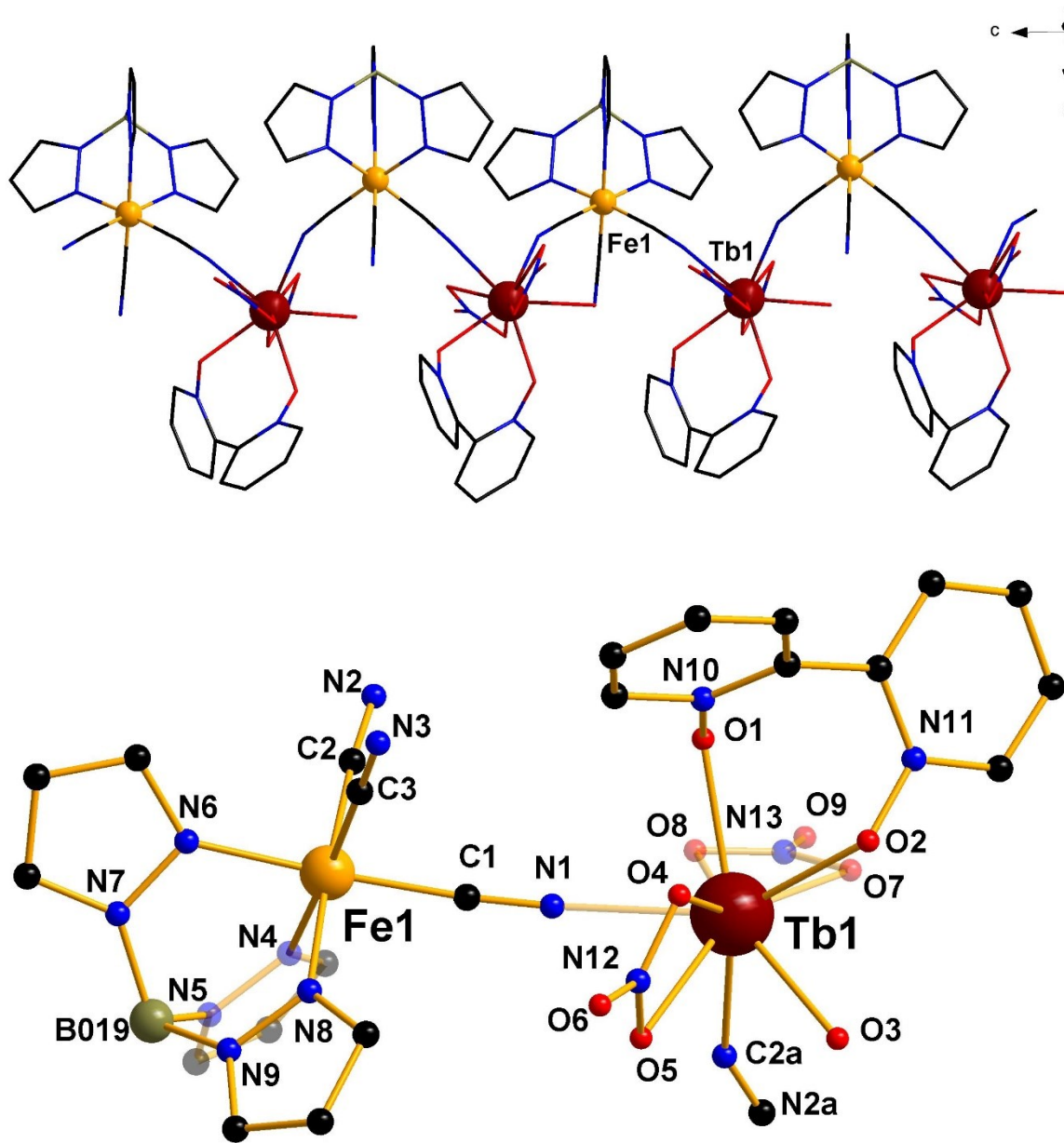


Fig. S9. (Top) View of a fragment of the cyanido-bridged $\{\text{Fe}^{\text{III}}\text{Tb}^{\text{III}}\}$ heterobimetallic chain in **2**. (Bottom) Asymmetric unit in **2** together with the atom numbering scheme [Symmetry code: (a) = $x, -1/2-y, -1/2+z$].

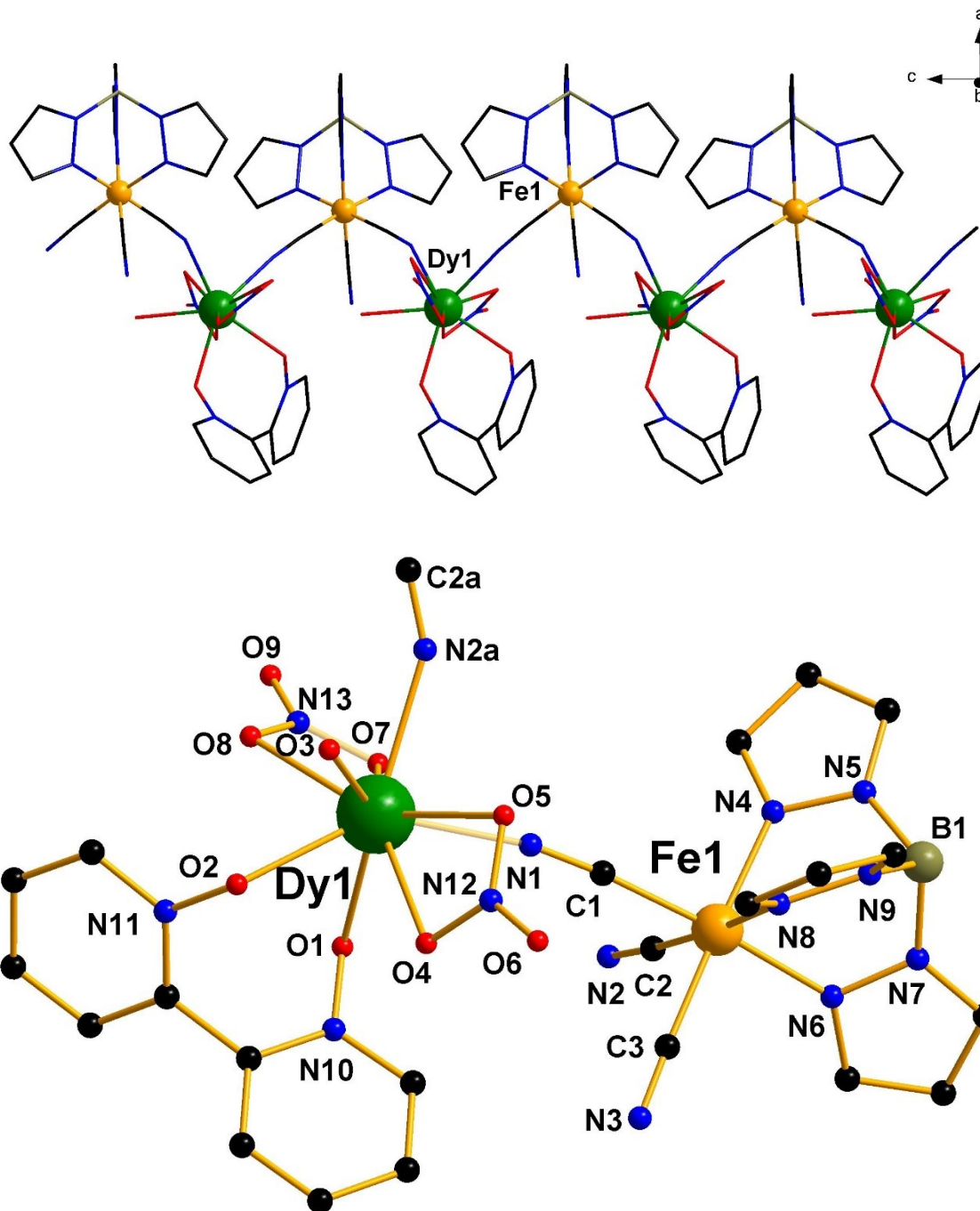


Fig. S10. (Top) View of a fragment the cyanido-bridged $\{\text{Fe}^{\text{III}}\text{Dy}^{\text{III}}\}$ heterobimetallic chain in **3**. (Bottom) Asymmetric unit in **3** together with the atom numbering scheme [Symmetry code: $(a) = x, 3/2-y, 1/2+z$].

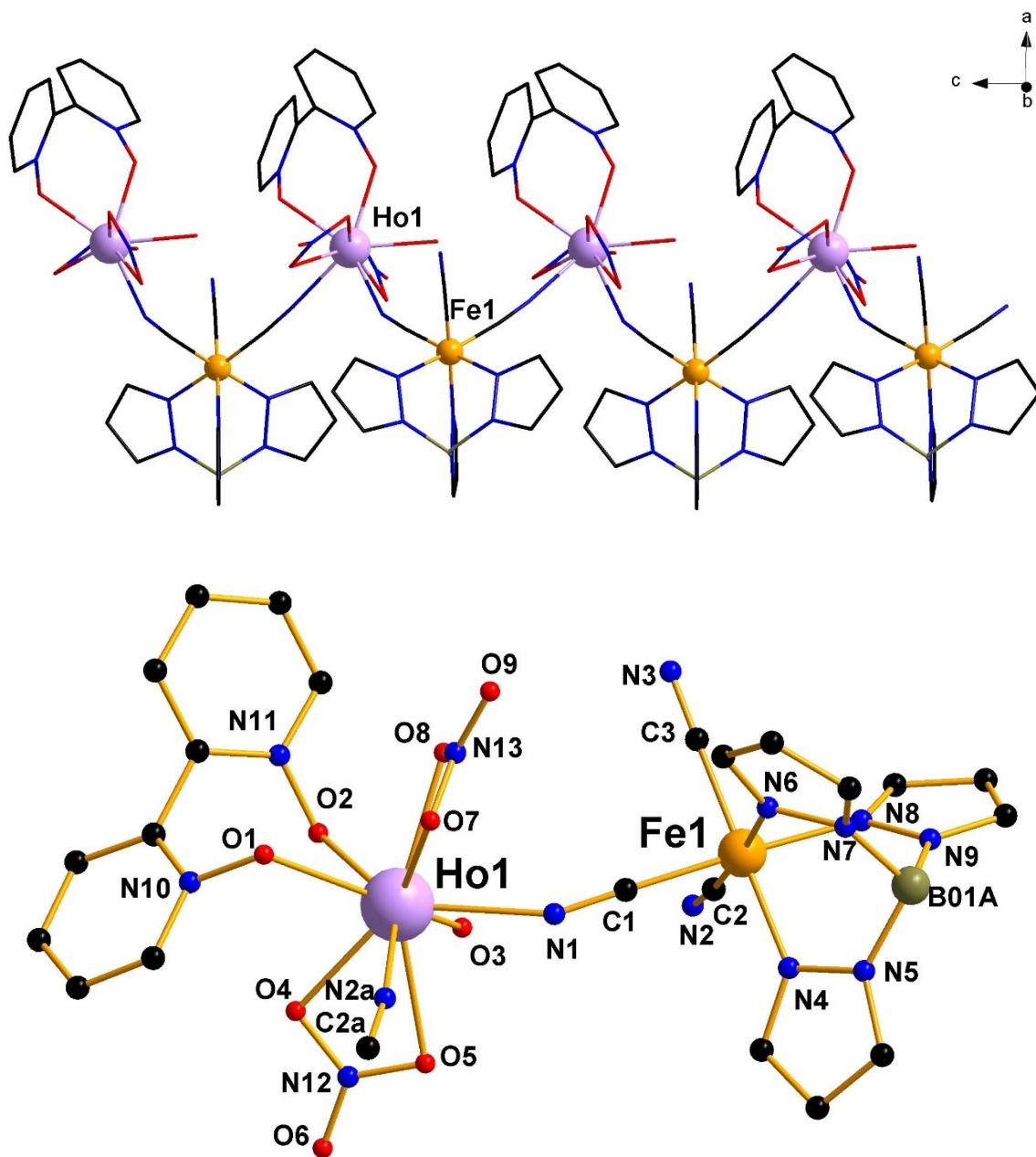


Fig. S11. (Top) View of the cyanido-bridged $\{\text{Fe}^{\text{III}}\text{Ho}^{\text{III}}\}$ heterobimetallic chain in **4**. (Bottom) Asymmetric unit in **4** together with the atom numbering scheme [Symmetry code: $(a) = x, -1/2-y, 1/2+z$].

Table S1. Bond Lengths (Å) and Angles (°) of the environments of the iron(III) and lanthanide(III) ions in **1-4***.

	1	2	3	4		1	2	3	4
Fe1-N4	1.985(7)	1.977(6)	1.977(5)	1.980(4)	N1-Ln1-N2a*	85.1(3)	84.6(2)	84.64(19)	84.78(15)
Fe1-N6	1.975(7)	1.971(6)	1.968(5)	1.972(4)	O1-Ln1-O2	71.5(2)	71.8(2)	71.60(17)	71.96(14)
Fe1-N8	1.955(7)	1.963(6)	1.965(5)	1.962(4)	O4-Ln1-O5	50.8(2)	51.43(19)	52.09(17)	51.80(12)
Fe1-C1	1.922(9)	1.922(8)	1.920(6)	1.921(5)	O7-Ln1-O8	51.7(2)	51.91(19)	51.50(16)	52.66(13)
Fe1-C2	1.905(9)	1.919(8)	1.911(7)	1.913(5)	O1-Ln1-N1	143.0(2)	142.8(2)	144.39(17)	143.00(14)
Fe1-C3	1.938(9)	1.939(8)	1.922(6)	1.934(6)	O1-Ln1-N2a*	78.6(2)	78.7(2)	78.80(17)	78.64(14)
Ln1-N1	2.475(8)	2.457(6)	2.448(5)	2.434(4)	O1-Ln1-O3	139.1(2)	139.5(2)	139.15(18)	139.28(13)
Ln1-N2a*	2.469(7)	2.453(7)	2.445(6)	2.433(4)	O1-Ln1-O4	78.2(2)	78.32(19)	75.29(16)	78.46(13)
Ln1-O1	2.413(6)	2.404(6)	2.388(5)	2.376(4)	O1-Ln1-O5	122.1(2)	122.42(19)	122.65(16)	122.96(13)
Ln1-O2	2.382(6)	2.367(6)	2.352(5)	2.351(4)	O1-Ln1-O7	71.4(2)	71.16(19)	71.29(16)	71.25(13)
Ln1-O3	2.433(7)	2.412(6)	2.401(5)	2.394(4)	O1-Ln1-O8	84.8(2)	84.8(2)	85.01(17)	85.32(14)
Ln1-O4	2.447(7)	2.441(6)	2.451(5)	2.400(4)	O2-Ln1-N1	130.5(2)	130.8(2)	130.95(18)	130.85(14)
Ln1-O5	2.547(7)	2.545(6)	2.532(5)	2.523(4)	O2-Ln1-N2a*	144.4(2)	144.6(2)	143.35(18)	144.35(14)
Ln1-O7	2.480(7)	2.472(6)	2.468(5)	2.455(4)	O2-Ln1-O3	68.9(2)	69.0(2)	68.84(17)	68.60(14)
Ln1-O8	2.485(7)	2.475(6)	2.422(5)	2.435(4)	O2-Ln1-O4	74.9(2)	74.51(18)	75.29(16)	74.38(13)
					O2-Ln1-O5	111.8(2)	112.03(18)	111.89(16)	111.98(12)
N4-Fe1-N6	88.8(3)	89.1(3)	88.9(2)	88.80(17)	O2-Ln1-O7	116.3(2)	116.45(19)	116.64(16)	117.08(13)
N4-Fe1-N8	87.7(3)	88.5(3)	88.2(2)	88.19(17)	O2-Ln1-O8	75.1(2)	75.07(19)	75.29(16)	75.24(13)
N6-Fe1-N8	88.2(3)	88.4(2)	88.5(2)	88.63(17)	O3-Ln1-N1	74.7(3)	74.6(2)	74.64(16)	74.65(14)
Fe1-C1-N1	175.6(7)	175.3(7)	175.3(6)	174.8(5)	O3-Ln1-N2a*	132.4(2)	132.2(2)	132.27(17)	132.18(14)
Fe1-C2-N2a*	174.9(8)	175.3(6)	175.3(6)	174.9(4)	O3-Ln1-O4	81.8(2)	81.8(2)	82.02(18)	81.64(14)
Fe1-C3-N3	178.9(8)	179.0(8)	177.9(6)	178.1(5)	O3-Ln1-O5	65.9(2)	65.89	65.77(17)	65.72(13)
C1-Fe1-C2	84.9(3)	84.9(3)	84.7(2)	85.2(2)	O3-Ln1-O7	137.2(2)	137.2(2)	137.31(18)	137.41(14)
C1-Fe1-C3	89.3(4)	86.9(3)	86.9(3)	89.4(2)	O3-Ln1-O8	94.8(2)	94.6(2)	94.47(18)	94.08(14)
C2-Fe1-C3	86.7(4)	89.4(3)	89.3(3)	86.6(2)	O4-Ln1-N1	131.5(2)	131.4(2)	131.00(18)	131.09(14)
N4-Fe1-C1	90.4(3)	90.2(3)	90.5(2)	90.46(19)	O4-Ln1-N2a*	80.4(2)	80.1(2)	80.37(18)	80.44(14)
N4-Fe1-C2	95.3(3)	95.2(3)	95.2(2)	95.3(2)	O4-Ln1-O7	140.9(2)	140.92(19)	140.56(16)	140.83(13)
N4-Fe1-C3	178.0(3)	177.7(3)	177.8(2)	178.1(2)	O4-Ln1-O8	148.9(2)	148.54(19)	148.89(17)	148.74(13)
N6-Fe1-C1	95.2(3)	94.9(3)	94.8(2)	94.44(19)	O5-Ln1-N1	80.8(2)	80.8(2)	79.58(18)	79.39(14)
N6-Fe1-C2	175.9(3)	175.7(3)	175.9(3)	175.9(2)	O5-Ln1-N2a*	68.6(2)	68.41(19)	68.54(17)	68.33(13)
N6-Fe1-C3	89.2(3)	88.7(3)	89.0(2)	89.34(19)	O5-Ln1-O7	131.7(2)	131.33(19)	131.29(16)	130.78(13)
N8-Fe1-C1	176.1(3)	176.4(3)	176.4(2)	176.6(2)	O5-Ln1-O8	153.1(2)	152.8(2)	152.33(17)	151.71(14)
N8-Fe1-C2	91.9(3)	91.9(3)	92.1(2)	91.88(19)	O7-Ln1-N1	71.8(2)	72.0(2)	72.36(17)	72.03(14)
N8-Fe1-C3	92.6(3)	92.0(3)	92.1(2)	89.34(19)	O7-Ln1-N2a*	70.0(2)	69.9(2)	69.88(18)	69.87(14)
Ln1-N1-C1	152.6(7)	151.5(6)	169.2(5)	151.9(4)	O8-Ln1-N1	75.9(3)	76.2(2)	76.37(19)	76.07(15)
Ln1-N2a-C2a*	169.0(7)	169.0(6)	151.4(5)	169.8(4)	O8-Ln1-N2a*	121.7(2)	121.8(2)	121.90(18)	122.45(14)

*Symmetry code: (a) = x, 3/2-y, -1/2+z (**1**); (a) = x, -1/2-y, 1/2+z (**2**); (a) = x, 3/2-y, -1/2+z (**3**); (a) = x, -1/2-y, -1/2+z (**4**)

Table S2. Summary of SHAPE analysis for the [LnN₂O₇] fragment in **1-4** [Ln = Gd (**1**), Tb (**2**), Dy (**3**) and Ho(**4**)]^a

CN = 9 ^b	Gd(III)	Tb(III)	Dy(III)	Ho(III)
EP-9	33.348	33.201	33.208	33.249
OPY-9	20.902	21.010	21.009	21.006
HBPY-9	16.226	16.300	16.330	16.494
JTC-9	14.848	14.850	14.773	14.785
JCCU-9	9.249	9.179	9.289	9.271
CCU-9	8.105	8.054	8.168	8.159
JCSAPR-9	3.375	3.303	3.258	3.214
CSAPR-9	2.371	2.317	2.273	2.235
JTCTPR-9	3.098	3.006	2.972	2.865
TCTPR-9	2.277	2.235	2.198	2.121
JTDIC-9	13.130	13.189	13.116	13.271
HH-9	8.958	8.943	9.097	9.081
MFF-9	2.206	2.165	2.154	2.119

^aThe listed values correspond to the deviation between the ideal and real coordination polyhedra, the lowest values being given in bold. ^bEP-9, *D*_{9h}, enneagon; OPY-9, *C*_{8v}, octagonal pyramid; HBPY-9, *D*_{7h}, heptagonal bipyramid; JTC-9, *C*_{3v}, Johnson triangular cupola J3; JCCU-9, *C*_{4v}, capped cube J8; CCU-9, *C*_{4v}, spherical-relaxed capped cube; JCSAPR-9, *C*_{4v}, capped square antiprism; CSAPR-9, *C*_{4v}, spherical capped square antiprism; JTCTPR-9, *D*_{3h}, tricapped trigonal prism J51; TCTPR-9, *D*_{3h}, spherical tricapped trigonal prism; JTDIC-9, *C*_{3v}, tridiminished icosahedron; HH-9, *C*_{2v}, hula-hoop; MFF-9, *C*_s, muffin.

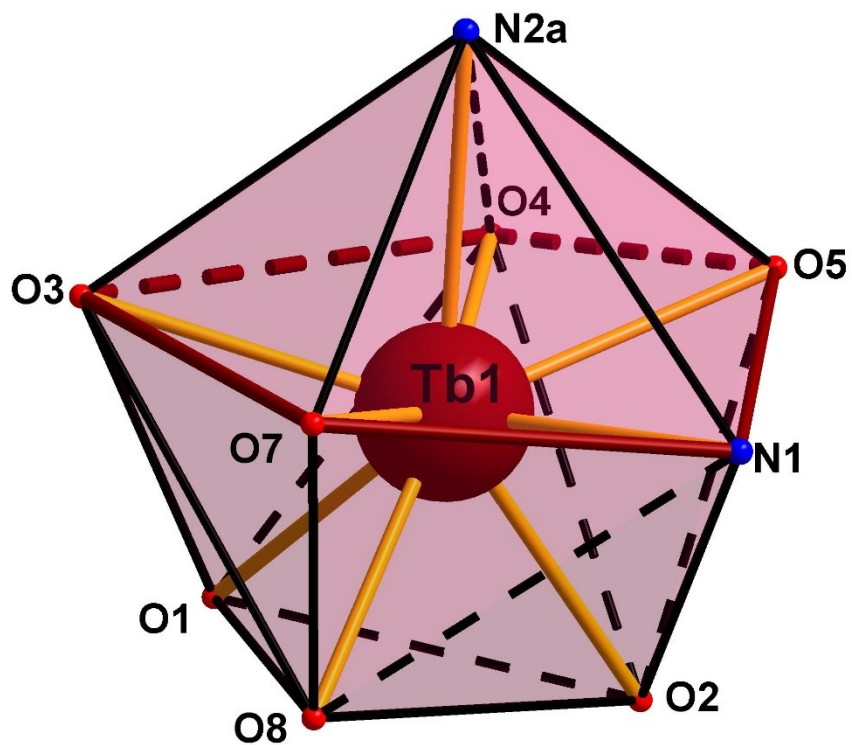


Fig. S12. Distorted mufin-like geometry for the terbium(III) ion in 2.

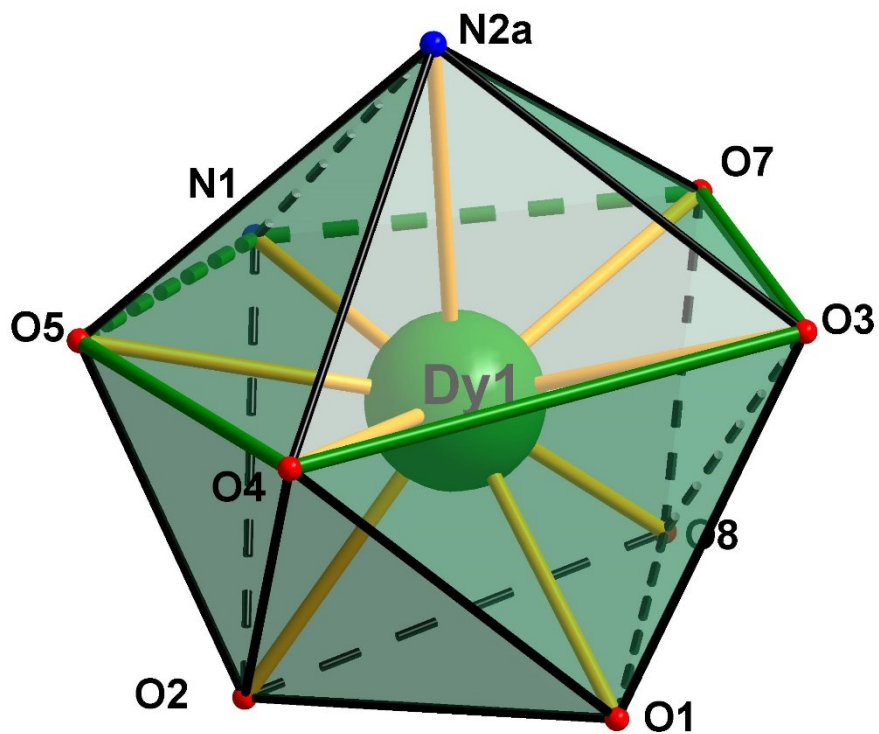


Fig. S13. Distorted mufin-like geometry for the dysprosium(III) ion in 3.

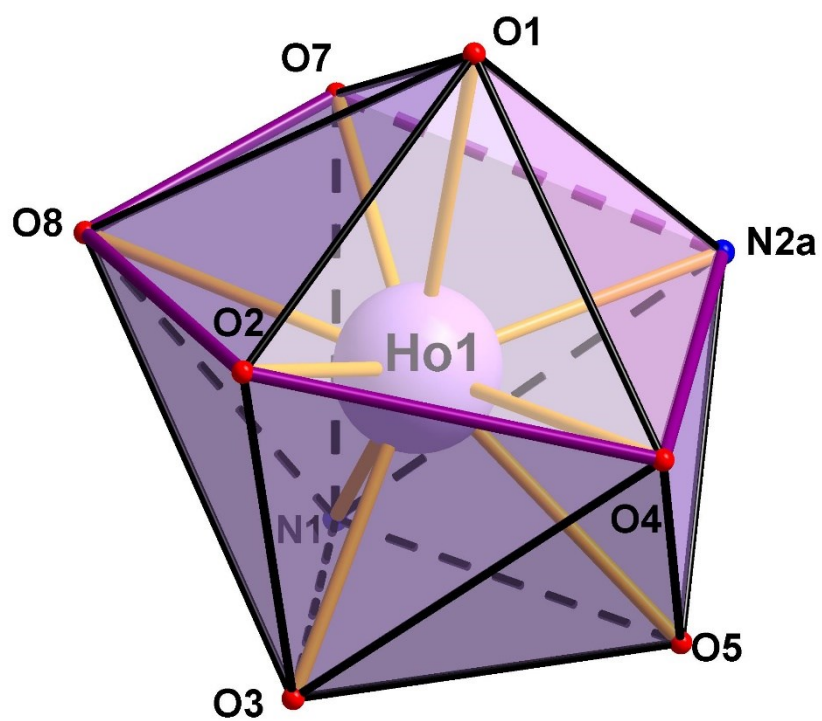


Fig. S14. Distorted mufin-like geometry for the holmium(III) ion in **4**.

Table S3. Selected intermolecular contacts (Å, deg) for **1-4**.

D-H...A	D-H (Å)	H...A (Å)	D...A (Å)	Angle D-H...A
1ⁱ				
O3-H3B...O1a	0.85	2.04	2.726(9)	137
O3-H3A...O7a	0.85	2.25	2.899(10)	133
2ⁱⁱ				
O3a-H3B...O1	0.86	2.00	2.731(8)	143
O3a-H3A...O7	0.83	2.20	2.910(8)	144
3ⁱⁱⁱ				
O3a-H3B...O1	0.89	2.01	2.745(7)	140
O3a-H3A...O7	0.85	2.33	2.923(7)	127
4^{iv}				
O3-H3A...O1a	0.85	2.00	2.744(6)	145
O3-H3B...O7a	0.86	2.39	2.921(6)	120

ⁱ(a) = x, 3/2-y, -1/2+z; ⁱⁱ(a) = x, -1/2-y, -1/2+z; ⁱⁱⁱ(a) = x, 3/2-y, 1/2+z; ^{iv}(a) = x, -1/2-y, -1/2

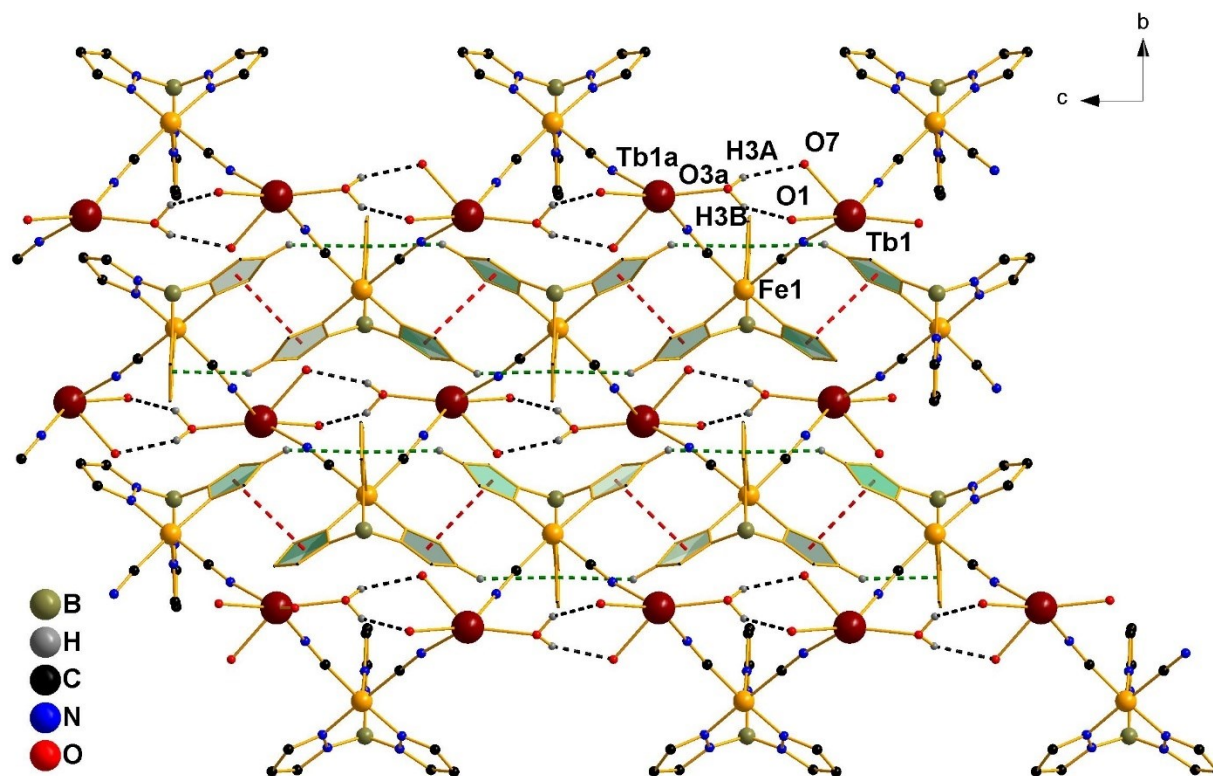


Fig. S15. View of a fragment of the packing diagram of **2** showing the supramolecular layer assembled in the crystallographic *bc* plane through C-H \cdots π (green-dotted lines) and slipped-off π - π (red-dotted lines) stacking interactions established between pyrazolyl rings of the HB(pz)₃⁻ ligands. The intrachain O3a \cdots O1 and O3a \cdots O7 hydrogen bonds are also represented as black-dotted lines [symmetry code: (*a*) = *x*, -1/2-*y*, -1/2+*z*]. The bdpo (except for the O1 donor atom), the terminal cyanide, nitrate (except for the O7 donor atom) and aqua ligands were removed for the sake of clarity.

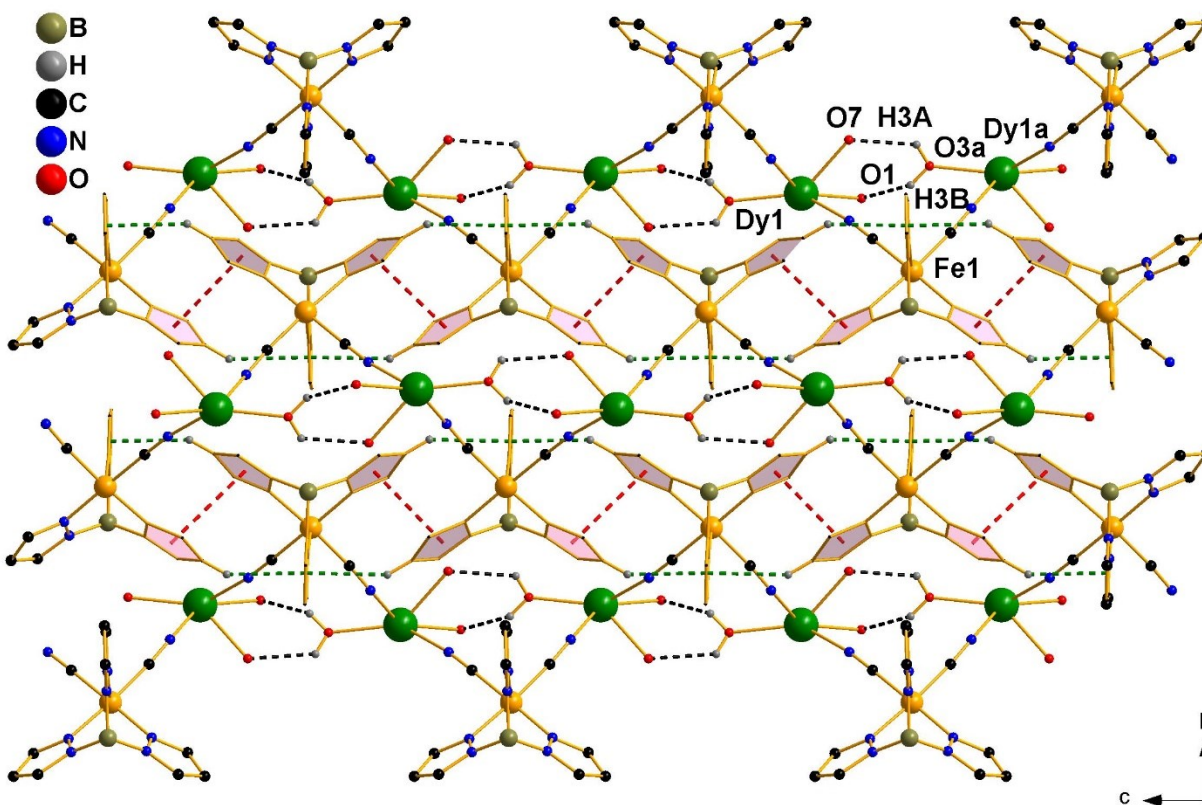


Fig. S16. View of a fragment of the packing diagram of **3** showing the supramolecular layer assembled in the crystallographic *bc* plane through C-H \cdots π (green-dotted lines) and slipped-off π - π (red-dotted lines) stacking interactions established between pyrazolyl rings of the HB(pz) $_3^-$ ligands. The intrachain O3a \cdots O1 and O3a \cdots O7 hydrogen bonds are also represented as black-dotted lines [symmetry code: (*a*) = *x*, 3/2-*y*, -1/2+*z*]. The bdpo (except for the O1 donor atom), the terminal cyanide, nitrate (except for the O7 donor atom) and aqua ligands were removed for the sake of clarity.

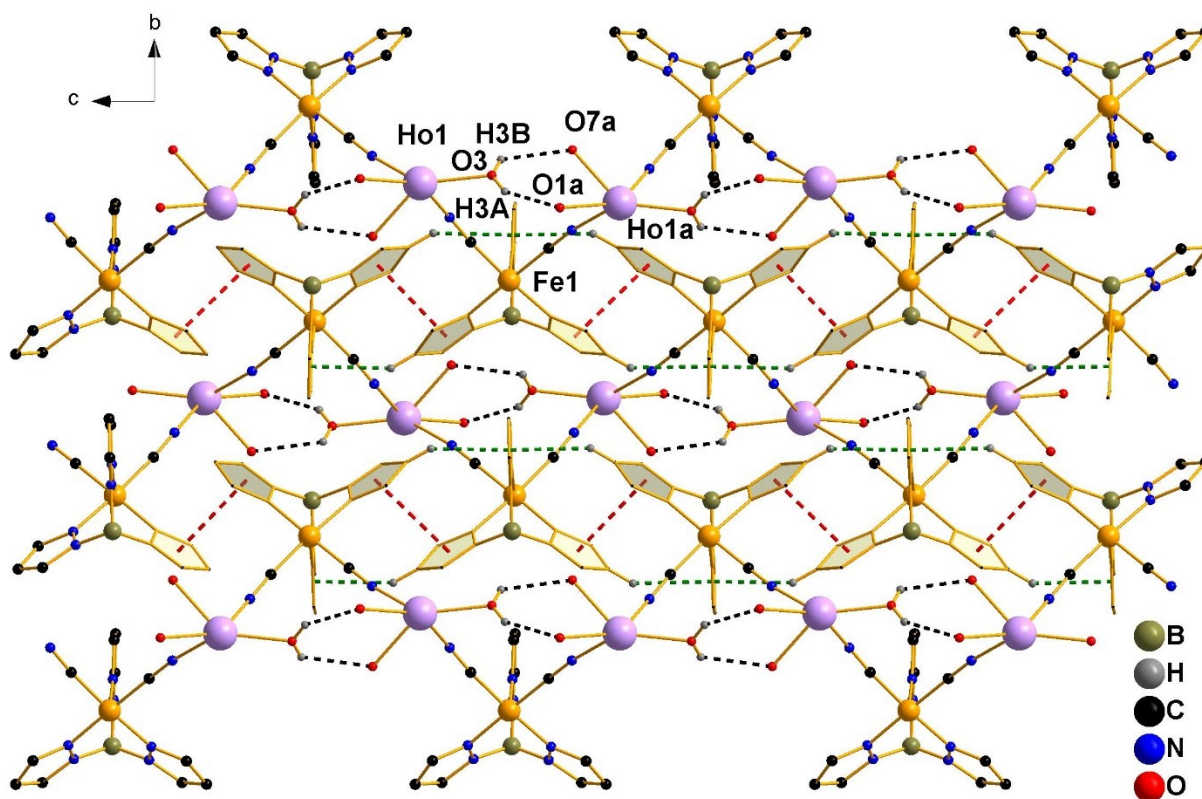


Fig. S17. View of a fragment of the packing diagram of **4** showing the supramolecular layer assembled in the crystallographic *bc* plane through C-H \cdots π (green-dotted lines) and slipped-off π - π (red-dotted lines) stacking interactions established between pyrazolyl rings of the HB(pz) $_3^-$ ligands. The intrachain O3 \cdots O1*a* and O3 \cdots O7*a* hydrogen bonds are also represented as black-dotted lines [symmetry code: (*a*) = *x*, -1/2-*y*, -1/2+*z*]. The bdpo (except for the O1 donor atom), the terminal cyanide, nitrate (except for the O7 donor atom) and aqua ligands were removed for the sake of clarity.

APPENDIX A

Magnetic susceptibility of an Alternating Ferrimagnetic Chain.

We consider the alternating local spins S_A and S_B with local Zeeman factors g_A and g_B and the interaction parameters between nearest neighbours $J_{AB}(1 + \alpha)$ and $J_{AB}(1 - \alpha)$. The corresponding spin Hamiltonian is given by eq 1B:

$$\hat{H} = -J \sum_i \hat{S}_{Bi} [(1 + \alpha) \hat{S}_{Ai} + (1 - \alpha) \hat{S}_{A(i+1)}] \quad (1B)$$

S_A is large enough to be treated as a classical spin and S_B is treated as a quantum spin. In our case $S_A = 1/2$ and $S_B = 7/2$. We define

$$J = J_{AB} [S_A(S_A + 1)]^{1/2}$$

$$G = g_A [S_A(S_A + 1)]^{1/2}$$

$$g = g_B ; S = S_B ; x = J/kT \quad (2B)$$

$$\chi_{Chain} = \frac{N\beta^2 g^2 [S(S + 1)(1 - P) + 2QR] + 2gG(Q + R) + G^2(1 + P)}{3kT(1 - P)} \quad (3B)$$

with

$$P = A_1/A_0$$

$$Q = x[(1 + \alpha)B_0 + (1 - \alpha)B_1]/A_0$$

$$R = x[(1 - \alpha)B_0 + (1 + \alpha)B_1]/A_0 \quad (4B)$$

and

$$A_0 = (2\pi/\Lambda^2) \sum_{\sigma=-S}^{+S} \sum_{\varepsilon=\pm} [\varepsilon \exp(i\sigma\varepsilon) (\sigma\lambda_\varepsilon)/\sigma^2] (\sigma\lambda_\varepsilon - 1)$$

$$A_1 = \left(\frac{\pi}{\Lambda^4}\right) \sum_{\sigma=-} \sum_{S\varepsilon=\pm}^{+S} [\varepsilon \exp(i\sigma\lambda_\varepsilon)/\sigma^4] [\sigma^3\lambda_\varepsilon^3 - 3\sigma^2\lambda_\varepsilon^2 + (6 - \sigma^2\lambda_\varepsilon^2)\sigma\lambda_\varepsilon + \sigma^2\lambda_\varepsilon^2 - 6]$$

$$B_0 = (2\pi/\Lambda^2) \sum_{\sigma=-} \sum_{S\varepsilon=\pm}^{+S} \varepsilon \exp(i\sigma\lambda_\varepsilon)$$

$$B_1 = \left(\frac{\pi}{\Lambda^4}\right) \sum_{\sigma=-} \sum_{S\varepsilon=\pm}^{+S} [\varepsilon \exp(i\sigma\lambda_\varepsilon)/\sigma^2] [\sigma^2\lambda_\varepsilon^2 - 2\sigma\lambda_\varepsilon + 2 - \sigma^2\lambda_\varepsilon^2] \quad (5B)$$

$$\text{being } \lambda_+ = -2x; \lambda_- = \alpha\lambda_+; \lambda^2 = 2x^2(1 + \alpha^2); \Lambda^2 = x^2(1 - \alpha^2) \quad (6B)$$

APPENDIX B [1]

Magnetic susceptibility of the 2T_2 term arising from the $(t_2)^1$ electronic configuration in a trigonally symmetric ligand field.

Using the methodology reported by Figgis² and Mabbs,³ the energy values obtained under the combined action of the spin-orbit coupling and a trigonal ligand field component [eq 1A] are given by eq 2A:

$$\hat{H} = \kappa\lambda\hat{L}\hat{S} + \hat{V}_{trigonal} \quad (1A)$$

$$E_1 = E_2 = \kappa\lambda(\nu - 0.5)$$

$$E_3 = E_4 = \frac{\kappa\lambda}{\sqrt{2}}a$$

$$E_5 = E_6 = \frac{\kappa\lambda}{\sqrt{2}}b \quad (2A)$$

ν being the distortion parameter defined as $\nu = \frac{\Delta}{\kappa\lambda}$ and

$$a = \frac{1}{\sqrt{2}}[(\nu + 0.5) - Z]$$

$$b = \frac{1}{\sqrt{2}}[(\nu + 0.5) + Z]$$

$$Z = \sqrt{\nu^2 + \nu + 2.25} \quad (3A)$$

The terms in the Hamiltonian which express the magnetic field perturbation for the parallel and perpendicular components are given by eq 4A. Because of the axial symmetry of the system, the x - and y -directions are identical.

$$\begin{aligned}\hat{H}_{Zeem,\parallel} &= \beta H(\kappa \hat{L}_z + 2\hat{S}_z) \\ \hat{H}_{Zeem,\perp} &= \beta H(\kappa \hat{L}_x + 2\hat{S}_x)\end{aligned}\quad (4A)$$

The first- and second-order Zeeman energies for the parallel and perpendicular directions are given in the Tables A1 and A2, respectively.

Table A1. First- and second Zeeman coefficients in the parallel direction.

E_i^0	$E_{iz}^{(1)}/\beta$	$E_{iz}^{(2)}/\beta$
$E_1 = E_2$	$\pm \kappa - 1$	0
$E_3 = E_4$	$\pm \frac{\kappa + 1 - a^2}{1 + a^2}$	$\frac{2(\kappa + 1 - ab)^2}{\kappa\lambda(1 + a^2)(1 + b^2)Z}$
$E_5 = E_6$	$\pm \frac{\kappa + 1 - b^2}{1 + b^2}$	$\frac{-2(\kappa + 1 - ab)^2}{\kappa\lambda(1 + a^2)(1 + b^2)Z}$

Table A2. First- and second Zeeman coefficients in the perpendicular direction.

E_i^0	$E_{ix}^{(1)}/\beta$	$E_{ix}^{(2)}/\beta$
$E_1 = E_2$	0	$\frac{2(\sqrt{2} - \kappa a)^2}{\lambda(1 + a^2)(\nu - 1.5 - Z)} + \frac{2(\sqrt{2} - \kappa b)^2}{\lambda(1 + b^2)(\nu - 1.5 - Z)}$
$E_3 = E_4$	$\pm \frac{\kappa a\sqrt{2} - a^2}{(1 + a^2)}$	$\frac{[\kappa(a + b) - ab\sqrt{2}]^2}{\kappa\lambda Z(1 + a^2)(1 + b^2)} - \frac{2(\sqrt{2} - \kappa a)^2}{\kappa\lambda(1 + a^2)(\nu - 1.5 - Z)}$
$E_5 = E_6$	$\pm \frac{\kappa b\sqrt{2} - b^2}{(1 + b^2)}$	$-\frac{[\kappa(a + b) - ab\sqrt{2}]^2}{\kappa\lambda Z(1 + a^2)(1 + b^2)} + \frac{2(\sqrt{2} - \kappa b)^2}{\kappa\lambda(1 + b^2)(\nu - 1.5 - Z)}$

From the above Zeeman coefficients and using the Van Vleck's equation, the parallel and perpendicular components of the magnetic susceptibility can be obtained (eqs 5A and 6A).

$$\chi_{\parallel} = \frac{N\beta^2}{kT} \frac{[E_{1z}^{(1)}]^2 \exp(-E_1/kT) + \{[E_{3z}^{(1)}]^2 - kTE_{3z}^{(2)}\} \exp(-E_3/kT) + \{[E_{5z}^{(1)}]^2 - kTE_{5z}^{(2)}\} \exp(-E_5/kT)}{\exp(-E_1/kT) + \exp(-E_3/kT) + \exp(-E_5/kT)} \quad (5A)$$

$$\chi_{\perp} = \frac{N\beta^2}{kT} \frac{-kTE_{1x}^{(2)} \exp(-E_1/kT) + \{[E_{3x}^{(1)}]^2 - kTE_{3x}^{(2)}\} \exp(-E_3/kT) + \{[E_{5x}^{(1)}]^2 - kTE_{5x}^{(2)}\} \exp(-E_5/kT)}{\exp(-E_1/kT) + \exp(-E_3/kT) + \exp(-E_5/kT)} \quad (6A)$$

The magnetic susceptibility for microcrystalline samples is determined through eqn 7A.

$$\chi_M = \frac{\chi_{\parallel} + \chi_{\perp}}{3} \quad (7A)$$

Refereces

1. M. Pacheco, A. Cuevas, J. González-Platas, R. Faccio, F. Lloret, M. Julve, C. Kremer, *Dalton Trans.*, 2013, **42**, 15361.
2. B. N. Figgis, *Trans. Faraday Soc.*, 1961, **57**, 198; (b) B. N. Figgis, *Nature*, 1958, **182**, 1568.
3. F. E. Mabbs and D. J. Machin, “*Magnetism and Transition Metal Complexes*”, Dover Publications, Inc., Mineola, NY, **2008**.